

VLT Spectroscopy of Galaxies Lensed by Abell AC114:

Implication for the Mass Model and the Study of Low-Luminosity Galaxies at High-Redshift *

L.E. Campusano¹, R. Pelló², J.-P. Kneib², J.-F. Le Borgne², B. Fort³, R. Ellis⁴, Y. Mellier^{3,5}, and I. Smail⁶

¹ Observatorio Cerro Calán, Dept. de Astronomía, U. de Chile, Casilla 36-D, Santiago, Chile

² Observatoire Midi-Pyrénées, UMR 5572, 14 Avenue E. Belin, F-31400 Toulouse, France

³ Institut d'Astrophysique de Paris, 98 bis boulevard Arago, 75014 Paris, France

⁴ Astronomy 105-24, Caltech, Pasadena CA 91125, USA

⁵ Observatoire de Paris, DEMIRM, 61 avenue de l'Observatoire, 75014 Paris, France

⁶ Department of Physics, University of Durham, South Road, Durham DH1 3LE, England

Received, 2001, Accepted, 2001

Abstract. We present the first results of a spectroscopic survey of faint lensed galaxies in the core of the galaxy cluster AC114 ($z=0.312$) obtained from observations with the FORS1 spectrograph mounted on the VLT-Antu (Unit Telescope 1). The galaxies were chosen in areas close to the high- z critical lines predicted by the gravitational lens model of Natarajan et al (NKSE, 1998) for this cluster, according to both lensing and photometric redshift criteria. All the target galaxies are found to correspond to background galaxies with redshifts values in the $[0.7, 3.5]$ interval. Our spectroscopic observations confirm the predicted lensing redshifts for 3 of the multiple-image galaxies, and together with predictions of the NKSE model led to the discovery of a new 5-image configuration at redshift $z = 3.347$. A revised NKS model, compatible with the redshift of this new multiple-image system, was generated and employed to calculate the gravitational amplifications of all the observed galaxies. The galaxies corresponding to the multiple-image systems are found to be intrinsically fainter, between 0.5 and 1.5 magnitudes, than the limiting magnitudes of existing *blank field* studies. When all the observed background galaxies are considered, the resulting intrinsic absolute magnitudes range from $M_B \sim -22$ to -19 , with a median value of -20.5 . Therefore, a large gain in sensitivity towards low luminosity high- z objects can actually be obtained, in agreement with theoretical expectations. This method can be used advantageously to probe the high redshift Universe and, in particular, its application to an ensemble of massive cluster cores could constraint the faint end of luminosity function of high redshift galaxies.

Key words. Cosmology: observations— Galaxies: clusters: individual(AC114)— Galaxies: fundamental parameters— gravitational lensing— Galaxies: redshifts – general – Methods: data analysis – spectroscopy

1. Introduction

The investigation of the properties of distant galaxies can be conducted by observing them either in *blank fields* or through the cores of massive clusters of galaxies. Clusters lenses are *natural telescopes* gravitationally magnifying the background galaxies, thus allowing the detection of intrinsically fainter and more distant galaxies than otherwise possible. Of particular interest, is the study of spectroscopically confirmed high- z galaxies in cluster cores where the amplification is the highest, attaining typically

values from 1 to 3 magnitudes. A sample of these galaxies would extend to fainter magnitudes than the ones currently available from surveys of the field (Steidel et al 1996a, 1996b, 1998, 1999), and also complement the latter, because it would be less biased towards intrinsically brighter galaxies. Therefore, this approach can be used with great advantage to find still higher redshift galaxies and to probe the faint end of the luminosity function at high redshift.

Natural telescopes have been successfully used in studying distant galaxies at almost all wavebands from UV (Bézecourt et al 1999), Optical (*e.g.* Ebbels et al 1998; Pelló et al 1999a, 1999b), Mid-Infrared (Altieri et al 1999, Metcalfe et al 1999) to Submm (Smail et al 1997, Ivison et al 2000). A difficulty of the optical/near-infrared,

Send offprint requests to: L. Campusano e-mail: lcampusa@das.uchile.cl

* Based on observations collected with the ESO Very Large Telescope Antu (UT1) and NTT 3.5m Telescope, and the Hubble Space Telescope.

Fig. 1. *HST/WFPC2* image (F702W) of AC114 cluster core with the identified high redshift galaxies and multiple images. The thin contour lines represent the total mass distribution as modelled by Natarajan et al (1998). The critical lines (dotted lines) are shown for $z = 3.35$. Circles show the position of the observed E system, and crosses correspond to the positions predicted by the NKSE model for the counter images of E1.

much less critical in other wavebands, is the contamination by cluster galaxies which are not always easily separated from the background population. Furthermore, because of the shallow slope of the galaxy number counts at faint magnitude, the magnification effect dilutes the density of background galaxies in the visible/near-infrared bands, hence for a given magnitude limit, there will be effectively less galaxies seen through a cluster lens than in *blank fields* (Broadhurst 1995, Fort et al. 1997, Mayen & Soucail 2000). For the study the luminosity function of high redshift galaxies, a large number (typically ~ 100) of these galaxies are needed. Such number of galaxies, can be collected through observations, like the ones reported here, of a sample of about 10 massive cluster-lenses. Our selection criteria of the distant galaxy candidates are based on a combination of lensing (Kneib et al 1994, 1996; Ebbels et al 1998) and photometric redshift criteria (e.g. Mobasher et al 1996, Lanzetta et al 1996, Gwyn & Hartwick 1996, Sawicki et al 1997, Giallongo et al 1998, Fernández-Soto et al 1999, Arnouts et al. 1999, Furusawa et al 2000, Bolzonella et al 2000). Although the lensing criteria in the cluster core is sufficient (once the mass distribution of the cluster is well determined) for the selection of distant galaxies (Ebbels et al 1998), photometric redshifts are very effective to select them in the outer part of the cluster and are also essential in identifying distant galaxies not resolved by *HST* and located in the cluster core. Furthermore, the photometric properties of the faint galaxies helps to optimise the instrument choice for the spectroscopic follow-up (visible vs. near-IR bands).

In this paper, we focus on a particularly interesting cluster-lens, AC114 (also named ACO S1077, Abell et al 1989), a $z=0.312$ rich cluster showing a large number of multiple-images at high- z (Smail et al 1995; Natarajan et al 1998, hereafter NKSE). The redshift of the gravitational pair S1/S2, $z = 1.86$, was obtained by Smail et al. (1995) with AAT, and later confirmed with NTT with a total exposure time of ~ 10 hours. Based on this redshift, the detailed mass-model derived by NKSE predicts the redshifts of 4 multiple images (*A, B, C* and *D*), ranging from $z \sim 1$ to 2.5. Here, we present the results obtained from a spectroscopic survey of lensed galaxies in AC114 conducted with VLT/FORS1 at Paranal (program 64.O-0439A). Sections 2 and 3 present a summary of the observations, selection criteria and data reduction. A detailed discussion of the spectroscopic results is given in Section 4. In Section 5, we briefly discuss the improved lens model for AC114, which now includes the spectroscopic redshift of 2 multiple images as constraints. The properties of these amplified galaxies are described in Section 6. Discussion

Table 1. Characteristics of the images and detection levels. 3σ magnitudes correspond to objects with 4 connected pixels, each 3σ above the sky level. Observations were carried out at the *HST* (1), ESO NTT (2), the CTIO 4m telescope (3) and the the AAT (4).

	t_{exp} (ksec)	σ (")	pix (")	λ_{eff} (nm)	$\Delta\lambda$ (nm)	m 3σ	Ref.
U	20.0	1.3	0.36	365	40	27.1	a, 3
B	9.0	1.2	0.39	443	69	27.7	4
V	21.6	1.1	0.47	547	53	26.7	b, 2
V_{555}	20.7	0.3	0.10	545	105	25.8	b, 1
R	16.8	0.13	0.10	694	122	25.7	c, 1
I_{814}	20.7	0.3	0.10	801	134	24.9	b, 1
J	7.2	0.9	0.29	1253	169	21.5	2
K'	10.8	0.8	0.29	2164	164	20.0	2

a) Barger et al 1996

b) Smail et al 1991

c) Natarajan et al 1998

and conclusions are given in Sections 7 and 8. Throughout this paper, we adopt $H_0 = 50 \text{ km s}^{-1} \text{ Mpc}^{-1}$, $\Omega_m = 0.3$ and $\Omega_\Lambda = 0.7$.

2. Imaging data and target selection

All the publicly available images of the cluster core of AC114, to October 1999, were employed for the selection of background galaxies. These data include deep *HST* images in 3 filter bands: F555W/*WFPC* (V_{555}), F702W/*WFPC2* (R), and F814W/*WFPC* (I_{814}), as well as U (CTIO) and V (ESO-NTT) images. In addition, we used deep imaging from a related program with ESO-NTT and the SOFI camera, including both J and K bands. Unfortunately, a photometric run with SUSI, aimed at obtaining B photometry, failed because of weather. After our VLT spectroscopic run, we got an existing deep B-image (courtesy of W. J. Couch), which is taken into consideration for the discussion about the photometric and lensing redshifts of the spectroscopically observed galaxies. The basic characteristics of these images are listed in Table 1, including magnitude limits, and references.

In the very central part of the cluster, the high-redshift galaxy candidates were mainly selected using lensing criteria (eg NKSE). Photometric redshifts were primarily used for the selection of background galaxies lying on the outer part of the cluster core, where lensing criteria are much less efficient, as well as in the core for cases when lensing failed to give any prediction - specially when the image of the galaxy was barely resolved. The photometric

catalogue was constructed, after matching the seeing values on the different images, using the SExtractor package (Bertin & Arnouts 1996). Magnitudes in this paper refer to the Vega system. Photometric redshifts (hereafter z_{phot}) were computed through a standard minimization procedure, using the *hyperz* code (Bolzonella et al 2000). This procedure uses a template library of spectra mainly derived from the new Bruzual & Charlot evolutionary code (GISSEL98, Bruzual & Charlot 1993). Photometric redshifts were derived from magnitudes computed within a $4''$ diameter aperture. In the case of highly distorted images, located close to bright cluster members, such as A, B and C, photometry was obtained through special apertures adapted to the shape of each object so that the same physical region was considered for the magnitude calculations in all the available images. Because of the lack of a B-band image, the error bars of the photometric redshifts employed in the target selection were found to be typically $\sigma_z \sim \pm 0.2$ to 0.3 , with degenerate solutions in some cases. Given that the CCD images cover fields of different size, the photometric selection could be done effectively only on the central *HST* field covering $\sim 80'' \times 80''$. Twelve galaxy candidates, with $z \geq 1.0$ and $R < 24$ were identified in this region.

Given that both lensing and photometric redshifts were available for most of the high- z galaxy candidates lying in the cluster core, and that the spectroscopic set-up allowed the observation of only a few of them, we proceeded mostly with the candidates with consistent redshift predictions. The designation of the observed objects is the same as that of NKSE, when available, otherwise they are labelled "V" with numbers increasing with their distance from the cluster center. The galaxies in the core that were actually observed, are identified in Fig. 1. In Table 2, positions and UBVRIJK photometry are given for the all the observed background galaxies.

3. Spectroscopic Observations and data reduction

The spectra of the high-redshift galaxy candidates were obtained on the night of October 5, 1999, with the ESO VLT Antu (UT1) telescope and its FORS1 spectrograph working on the multi-object mode. A slit width of $1''$ and the grism G300V were used, resulting in a wavelength coverage of $\sim 4000\text{--}8600\text{\AA}$, and a resolution of $R = 500$. Three masks, or slit configurations, were employed for total exposure times of 2h15m, 1h30m and 1h17m, respectively. Each of them spans a $\sim 7'$ field, with 19 to 20 slitlets having a fixed $22''$ length. The fact that the slit length was comparable to the angular size of the cluster core, restricted to $\sim 5\text{--}6$ the number of strongly magnified galaxy candidates that could be observed per mask. Multiple images according to the NKSE model were given the first priority, and the secondary targets to fill the remaining slitlets inside the $1.2' \times 1.2'$ cluster core were chosen from the photometric high- z list of candidates. In order to improve the efficiency, we kept some of the faintest candidates from the cluster core in several slit configurations while changing

Fig. 2. Two dimensional spectra of background galaxies showing emission lines in the low redshift domain: $0.33 \leq z \leq 0.80$. Galaxies are identified as in Table 2. The arrows indicate the position of [OII]3727Å line. The wavelength interval 4760Å–6590Å is shown.

Fig. 3. Two dimensional spectra of background galaxies showing emission lines in the high redshift domain: $0.80 \leq z \leq 1.21$. Galaxies are identified as in Table 2. The arrows indicate the position of [OII] line at 3727Å. The wavelength interval 6620Å–8500Å is shown.

the brighter targets lying in the outer parts of the cluster. Once the priority targets had determined the position of the center of the mask and its orientation, the slits outside the core could be used only to observe galaxy cluster members. The seeing values during the observations were in the range $\sim 0.6\text{--}0.8''$, except during the last 1500 seconds of the exposure with the third mask ($1.3''$). Spectra of the spectrophotometric standard star Feige 110 were obtained during twilight for calibration. The data reduction was done using standard IRAF packages.

4. Spectroscopic Results

Sixty-two galaxy spectra were extracted from the integrations performed through the 3 mask configurations selected for use with FORS1. The inspection of the wavelength and flux calibrated spectra, revealed that twenty-seven were galaxies belonging to AC114, twenty-three galaxies lay in the background of the cluster, and ten were foreground galaxies (two spectra remained unidentified). In this paper, we concentrate on the spectroscopically identified background galaxies and, in particular, on those located in the central $1.2' \times 1.2'$ region of AC114. The results on the cluster galaxies will be presented in a forthcoming paper.

The 2-dimensional spectra of the background galaxies with $0.33 \leq z \leq 0.80$ are shown in Figure 3, where the arrows indicate the position of the [OII] line at 3727Å. Similarly, Figure 3, displays the 2-dimensional spectra for the $0.80 \leq z \leq 1.21$ interval. Figure 4 displays calibrated one-dimensional spectra of the observed background galaxies with $z \gtrsim 1$, showing the identified emission and absorption features. The designation of the galaxies is the same as indicated in Table 2.

The redshifts measured for the background galaxies are listed in Table 3, together with the identified spectral features either in absorption or emission. For the objects with a fair signal-to-noise value, the best fit galaxy spectral type is given, from E to Im. A discussion on the redshift determinations of the galaxies lying in the cluster core is given below, which is specially delicate for the spectra presenting only one strong spectral feature. Table 3 summarizes the redshift determinations and the main spectral features identified. Excepting one uncertain case (V1, see Sect.6.5), all of the 10 high- z candidates selected in the

Id.	r.a.(J2000.0)	dec.(J2000.0)	U	B	V	R	I_{814}	J	K'
A1	22:58:49.58	-34:47:53.0	23.72	23.37	22.35	23.07	23.32	22.07	21.43
A2	22:58:47.77	-34:48:04.							
B2	22:58:46.80	-34:47:54.8	23.66	24.02	23.28	22.48		22.54	22.25 :
B3	22:58:46.53	-34:47:57.1							
C3	22:58:46.11	-34:47:59.2	24.68	24.37	23.59	22.44	23.66	-	-
E1	22:58:46.67	-34:48:22.4	-	25.06	24.32	23.77	23.59	-	22.68
S2	22:58:48.78	-34:47:54.0	22.46	22.81	22.54	22.01	22.10	21.04	19.99
V1	22:58:50.59	-34:48:24.9	24.27	24.77	24.69	23.94	23.23	21.59	19.80
V2	22:58:50.72	-34:47:54.3	23.49	24.27	23.91	23.20	22.84	21.71	21.06
V3	22:58:51.61	-34:47:59.6	24.70	25.31	24.94	23.79	22.78	21.04	19.37
V4	22:58:44.39	-34:48:06.7	24.06	24.42	23.97	23.06	23.28	22.45	21.03
V5	22:58:45.75	-34:48:15.8	23.80	24.50	23.84	22.97	22.68	21.10	19.25
V6	22:58:50.94	-34:47:26.5		23.56	22.58	21.77	20.95	20.03	18.73
V7	22:58:45.60	-34:49:03.9	22.88	22.97	22.16	20.66	20.15	19.17	17.68
V8	22:58:54.12	-34:48:28.2		23.71				20.37	18.92
V9	22:58:56.56	-34:46:58.6		22.67					17.00
V10	22:58:56.98	-34:48:45.8		25.29					17.72
V11	22:58:57.46	-34:47:06.8		23.61					18.39
V12	22:58:38.15	-34:48:25.3		22.84		20.58		19.30	17.43
V13	22:58:38.70	-34:50:08.2		24.24				20.67	18.69
V14	22:58:38.71	-34:50:08.5		24.04				21.60	19.77
V15	22:58:36.21	-34:49:40.5		25.28					17.03
V16	22:58:34.59	-34:49:30.1		23.08					18.15
V17	22:58:34.80	-34:50:34.1		26.26					18.75
V18	22:58:33.65	-34:49:42.2		23.40					

Table 2. Position and photometry for the 23 observed background galaxies. The horizontal line separates the core sample, for which the strong selection criteria apply. When available, the identifications are given according to Natarajan et al 1998. "V" objects have numbers increasing with their distance from the cluster center. When a space is left blank, the object is "out of the field" in this filter, whereas non-detected objects are given by "-". V-band photometry corresponds to ground-based data. These are aperture magnitudes computed within a $4''$ -diameter aperture, after correction for seeing differences between the images.

cluster core region were found to have spectroscopic redshifts between ~ 1 and 3.5 , in good agreement with the redshift selection criteria. The strongly lensed galaxies in the cluster core are discussed one by one in Sect. 6.

For comparison, Table 5 lists the lensing (NKSE) redshifts for the multiple systems and the photometric redshifts for the the observed galaxies in the cluster core, all of them with predicted redshifts greater than ~ 1 . The only exception is V3, for which the *a posteriori* z_{phot} is lower than the initial estimate, $z \sim 0.8$, and in fair agreement with the spectroscopic value. Overall, our method to identify lensed galaxies with $z > 1.0$ had a success rate $\gtrsim 80\%$. Although the z_{phot} used for target selection had larger uncertainties than those given in Table 5 (because of the lack of deep B photometry), they were an effective complement to the z_{lens} specially in the case of barely resolved objects which did not have a predicted z_{lens} , and turned out to be fully compatible with the spectroscopic redshift within the errors. Table 5 also lists the z_{phot} for the rest of the observed background galaxies.

From Table 5, it can be seen that the z_{lens} predicted by the NKSE for A1/A2 is in remarkable agreement with the measured redshift for the system. Although the red-

shift determination of the systems B and C is more uncertain, they suggest that the z_{lens} predictions of the NKSE underestimate the actual values.

The object designated E1 in Table 3, showing a strong emission line with $z = 3.347$ when identified with $\text{Ly}\alpha$ (see Fig. 8), provided a surprising prediction of the NKSE lens model, which to a large extent was confirmed by the available data. E1, was selected as a high- z galaxy based solely on its photometric properties; it did not have a z_{lens} estimate because it appeared as an unresolved source. The NKSE mass model predicts that an object at the position of E1 with a redshift of 3.347 is one of the images of a 5 multiple-image lensing configuration. *A posteriori*, a close inspection of the *WFPC2* images reveals E1 as a compact unresolved component with a faint NW extension. The NKSE model predicted also the positions of the other four images: a close inspection of the *WFPC2* data showed the predicted images very close to the expected locations (see Fig. 1), all of them with a morphology similar to E1 (Figure 5) and possibly following the parity predicted by the lens model. Using E1, E2 and E5, the three images which are not contaminated by bright objects, we could verify, within the errors, that they actually have the

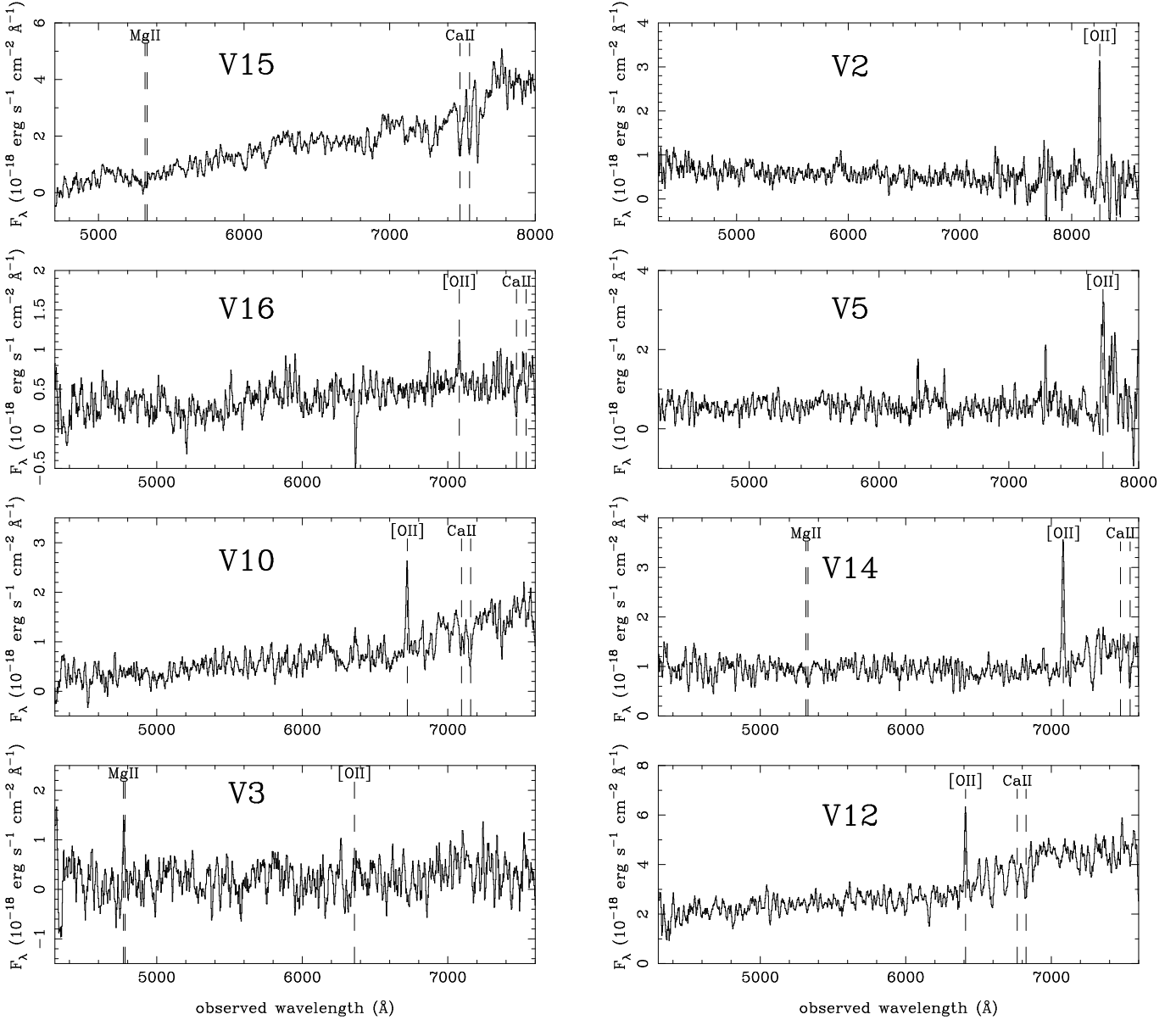


Fig. 4. Spectra of the identified galaxies in the background of AC114. The label on the top of each spectrum gives the identification number, according to Table 2, as well as the redshift. Spectra showing single emission lines are also displayed as 2D images. Fluxes are given in arbitrary units because of the lack of spectrophotometric conditions (neither the standard star nor the galaxy are well sampled by the slit), but they have the right order of magnitude in $\text{ergs s}^{-1} \text{cm}^{-2} \text{\AA}^{-1}$

same spectral energy distribution (SED), which is a necessary condition for gravitational images of the same source.

The discovery of the E-system, is a very impressive success of the NKSE mass model for AC114, but at the same time offers the possibility to improve the model. This is done in the next section.

5. The lensing mass model revisited

The NKSE lensing model has been revised in order to include the strong constraint imposed by the redshifts of two multiple-image systems: the 3-image S ($z = 1.86$),

that had been already included in the NKSE model, and the newly discovered 5-image E ($z = 3.347$).

We follow the NKSE assumptions in tuning up the mass model, and we refer to their work for more details. In summary, the mass distribution is well represented by a cluster-scale component, the central clump, and by an additional bimodal cluster-scale component, with the clumps centered on the main galaxy concentrations. A galaxy-scale component is also introduced, with galaxy halos centered on each bright cluster galaxy, modelled by a pseudo-isothermal elliptical mass distribution, with parameters scaled to the galaxy luminosity (truncation and core radius, velocity dispersion). To improve the optimisation of

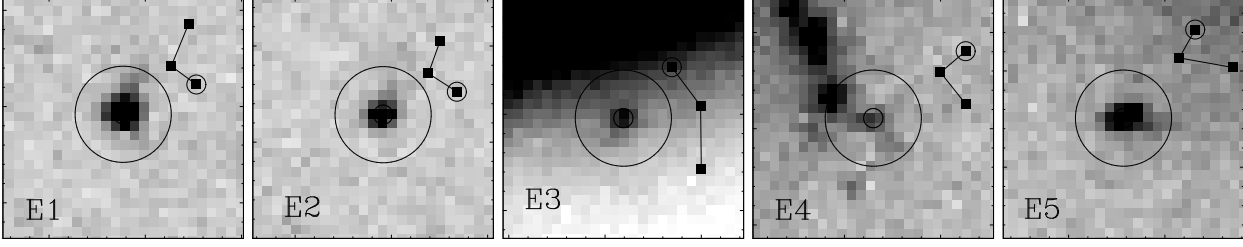


Fig. 5. Morphology of the 5 images of the multiple system E, labelled from E1 to E5. The size of each image is $2.5'' \times 2.5''$. We can identify on most images a point source with 2 faint extensions. At the top right of each panel, a representation is given to show the expected parity of the extensions for all five images. Although the image resolution is not good enough to confirm the prediction, it seems that the elongations on each images are as expected from the lensing theory.

Table 4. Characteristics of the new revised model for the mass distribution in AC114. For each mass component, the following parameters are given: position, ellipticity, core radius (r_c), velocity dispersion and truncation radius (r_t). The galaxy-scale component is given for L_B^* .

Mass Component	x (arcsec)	y (arcsec)	a/b	θ (deg)	r_c (kpc)	σ (km/s)	r_t (kpc)
Central Clump	0.0 ± 0.5	0.0 ± 0.5	2.1 ± 0.05	14.5 ± 0.5	97 ± 5	1036 ± 5	2000 ± 200
Clump 1	-105.0 ± 10	0.0 ± 10	1.25 ± 0.1	40 ± 10	100 (<i>fixed</i>)	620 ± 20	1000 (<i>fixed</i>)
Clump 2	80.0 ± 5	-35.0 ± 10	1.35 ± 0.1	-30 ± 10	100 (<i>fixed</i>)	450 ± 20	1000 (<i>fixed</i>)
L_B^* Galaxy halo	—	—	—	—	0.15	205 ± 5	25 ± 5

the *LENSTOOL* software (Kneib 1993), we used a new technique involving both a Monte-Carlo search as well as a parabolic minimization (Golse, Kneib, Soucail 2001). Only the positions of the multiple images were fitted, and the free model parameters were the ellipticity, orientation, velocity dispersion, core radius of the cluster clump, and the ellipticity, orientation, velocity dispersion and truncation radius of the central cD galaxy. Table 4 summarizes the characteristics of the new revised model for the mass distribution. The best reduced χ^2 found is ~ 2 .

Using the best fitted mass distribution, we checked that the mean measured differences in amplification agree with the ones observed. In particular for the E-system the measured values, $\Delta m_{E1-E2} = 0.1$ mags and $\Delta m_{E2-E5} = 0.7$ mags, are in good agreement with model predictions.

We also used the revised NKSE model to check the redshift prediction for the other multiple images in the cluster core. We found that the best redshift estimates for the multiple-image systems A, B, C and D are: $z_A = 1.7 \pm 0.05$, $z_B = 1.3 \pm 0.1$, $z_C = 2.3 \pm 0.1$ and $z_D = 1.4 \pm 0.1$. These values are larger than the ones previously predicted by NKSE (see Table 5), resulting in a better agreement between the z_{lens} and the spectroscopic redshifts (see Sect. 6).

Table 5 lists the lensing redshifts for the multiple-image systems observed with VLT in the cluster core, and the magnification prediction for the 23 background galaxies observed with FORS1, using the revised model of AC114 and the measured spectroscopic redshifts.

6. Lensed galaxies in the cluster core

The identification of spectral features and the main issues concerning multiple images and highly amplified galaxies are discussed in this section.

6.1. The multiple image A at $z=1.691$

In this case, the redshift is mainly based on a single emission line, which is found in both the spectra of A1 and A2 at 7518\AA . This line is identified as MgII (at 2798\AA), in good agreement with the shape of the continuum. Besides, the spectrum of A1 also displays absorption lines, mainly FeII(1608\AA) and AlII(1670\AA). A comparison between the spectra of A1 and the local starburst NGC4214 (Leitherer et al 1996) is given in Fig. 6. In addition, this redshift value is fully compatible with both the multiple-image configuration ($z = 1.7 \pm 0.05$ derived from the revised lensing model) and the z_{phot} (see Table 5). With $z=1.691$, we do not expect to find other strong emission lines, such as [OII] 3727\AA , CIV 1549\AA or Ly α , because they are outside the observed spectral range (Fig. 6).

6.2. The multiple image S at $z=1.867$

The previous determination of the redshift of the system S1/S2 by Smail et al (1995) is confirmed by the present results. We have obtained a spectrum for S2. Figure 7 displays the high S/N spectrum as well as the complete line identification. A detailed study on this particular object will be presented in a further paper. This object is also important because it allows a (positive) test of the z_{phot}

Id.	z (spectra)	Main Spectral features
A1	1.6912	MgII(2798Å), FeII(1608Å), AlII(1670Å)
A2	1.6912	e. line 7518Å
B2	1.50/2.08	e. line 4776Å
B3	1.50/2.08	e. line 4776Å
C3	2.84544	Ly α , CIV 1549Å
E1	3.34695	Ly α
S2	1.86710	blue cont., abs. lines (see text)
V1	?	no clear feature
V2	1.2143	Im, [OII]3727Å
V3	0.706	e. line 4776Å
V4	2.050	CIV 1549Å
V5	1.0726	S, e. line 7724.4Å
V6	0.40953	Im, [OII]3727Å, Balmer lines
V7	0.56692	Im, [OII]3727Å, [OIII]5007Å, Balmer lines
V8	0.58?	S, 4000Å break, faint abs. lines
V9	0.41205	Red S, [OII]3727Å, Balmer lines
V10	0.80340	Red S, [OII]3727Å, Balmer lines
V11	0.38048	Im, [OII]3727Å, [OIII]5007Å
V12	0.72002	S, [OII]3727Å, MgII, H, K,
V13	0.71965	S, [OII]3727Å
V14	0.90031	Im, [OII]3727Å, Balmer lines, MgII
V15	0.90233	E, H, K
V16	0.89935 ?	S, [OII]3727Å
V17	0.71169	S, H, K, Balmer lines
V18	0.8135 ?	Im, [OII]3727Å

Table 3. Redshift determination for the 23 observed background galaxies. The horizontal line separates the core sample, as in Table 2. For objects with fair S/N on the spectral continuum, the best fit spectral type is given, from E to Im.

techniques at $1 \leq z \leq 2$, a redshift domain which is particularly difficult to check because of the lack of strong spectral features.

6.3. A new multiple image system (E) at $z=3.347$

The initial redshift of the system was based on the spectrum taken for E1. The spectrum, shown in Fig. 8, shows a strong emission line which implies $z=3.347$ for the system when it is identified a Ly α line at 1216Å. As already mentioned, the use of this redshift and the mass model for AC114 predicted the additional 4 images of the system which are actually present with essentially the same morphology and SED. In fact, this system is one of the two new strong constraints of the new mass model presented in Sect. 5. Figure 9 shows the 2D spectra of E1 and A2+E4; E4 shows a very faint emission line at exactly the same wavelength as in E1, which is fully compatible with the lensing interpretation. The equivalent (rest frame) width of Ly α is $W_\lambda = 61 \pm 7$ Å. The error bar takes into account the uncertainties on the continuum level. The corrected absolute magnitude of the source galaxy, $M_B = -20.6$, to-

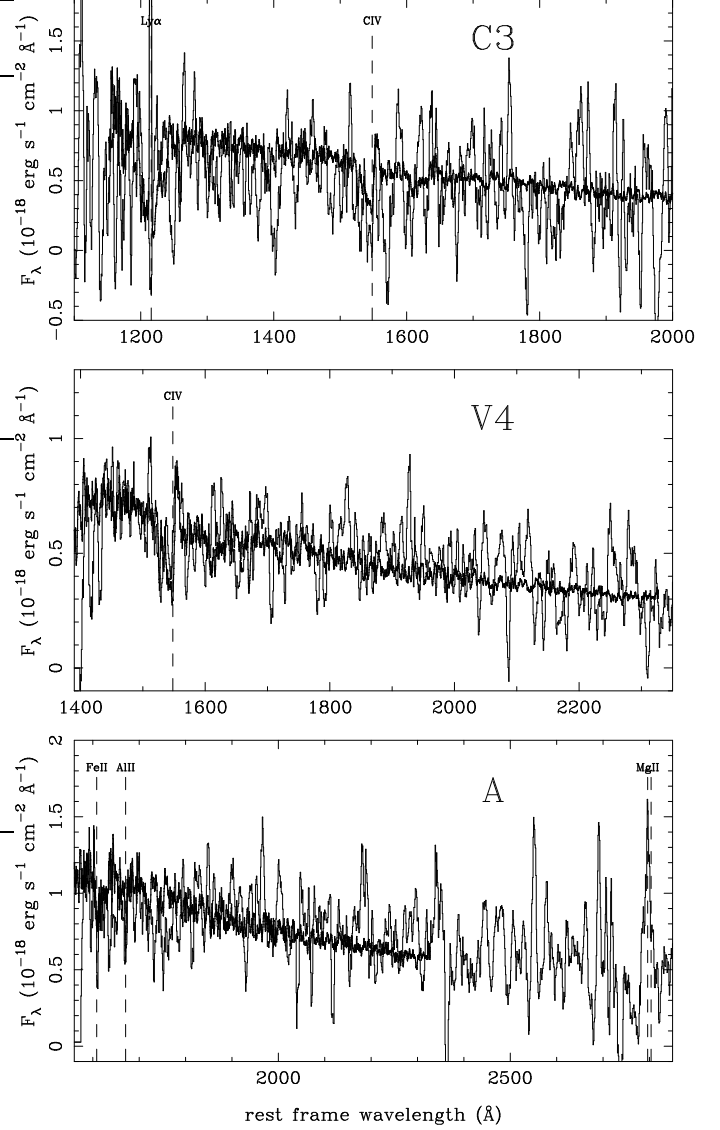


Fig. 6. From top to bottom, comparison between the spectra of C3 ($z=2.854$), V4 ($z=2.050$) and A1 ($z=1.691$) (thin lines), and the local starburst galaxy NGC4214 (Leitherer et al 1996) (thick lines). The main spectral features are shown.

gether with the observed morphology, suggests a Seyfert-like galaxy.

6.4. The multiple images B and C

We have obtained spectra for B2 and B3. A single emission line was found in both spectra, at $\lambda \sim 4776$ Å. Photometric redshift could be obtained only for B2 and B1 only, because B3 and B4 are contaminated by the neighbouring cluster galaxy on most of the ground-based images. The lensing and photometric redshifts for the image B2, are $z = 1.3 \pm 0.1$ and $z=1.61^{+0.19}_{-0.13}$, respectively, at 1σ . The z_{phot} for the image B1 is $z=1.57^{+0.26}_{-0.25}$, in excellent agreement with B2. The only plausible identification for the emission line satisfying these two conditions is CIII]1909Å,

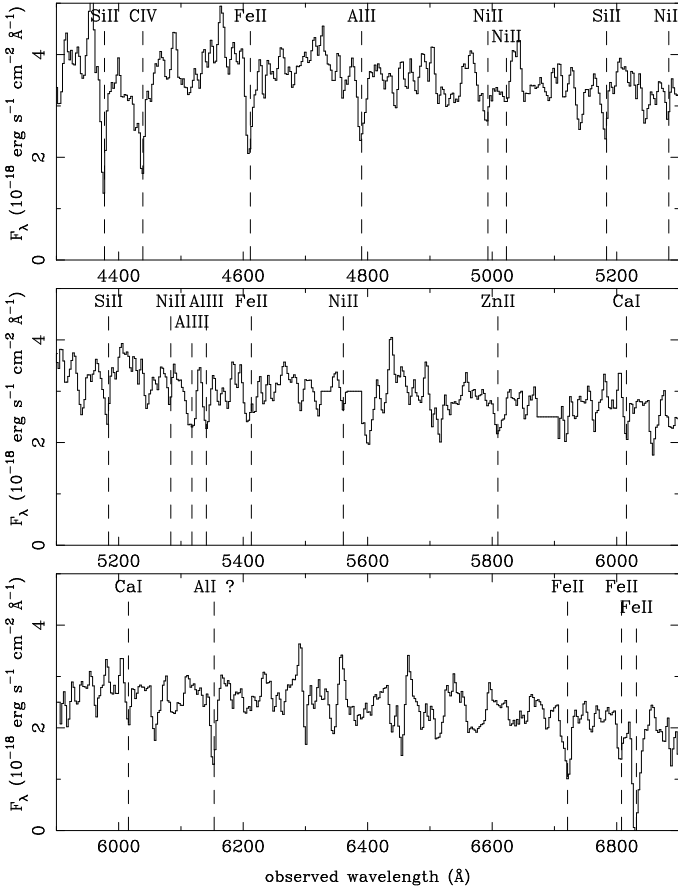


Fig. 7. Spectrum of object S2, at $z=1.867$, which confirms the identification of Smail et al 1995. Note the blue excess of this galaxy.

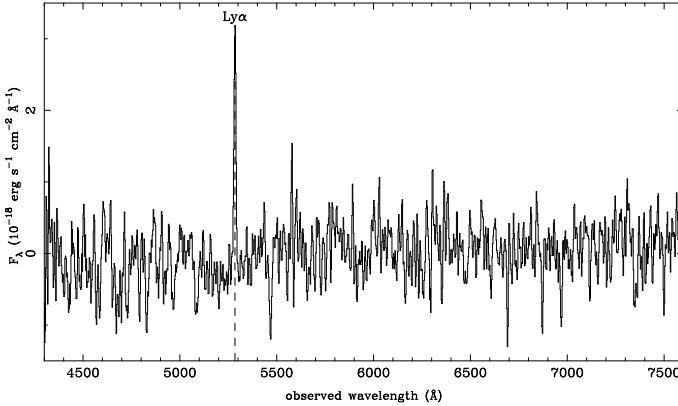


Fig. 8. Spectrum of object E1, at $z=3.347$, showing a strong emission line, identified as $\text{Ly}\alpha$. This redshift implies a 5-image system which is actually verified. No other features are clearly identified on the continuum.

implying a redshift of $z = 1.502$. However, it does not fit exactly with the lensing prediction suggesting that either the line identification is not correct, or the lens model in this region is not accurate enough. The emission line is seen on the spectra of both B2 and B3+B4, as can be appreciated in the 2D spectra shown in Fig. 10, thus it is likely to be a real feature. When it is identified with

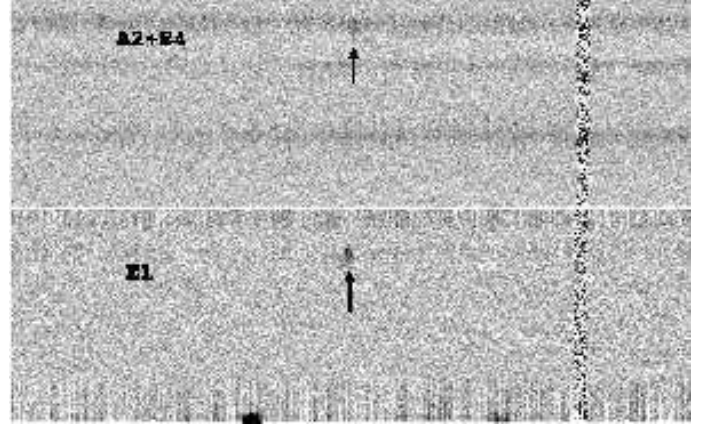


Fig. 9. Two dimensional spectra of two different images of the galaxy E. The arrows indicate the position of $\text{Ly}\alpha$ line. The spectrum of the image E4 is blended with that of image A2 of arc A, responsible for the spectral continuum seen. Note the slight shift along the slit between continuum spectrum of A2 and the emission line of E4, which is compatible with their position and orientation on the HST image.

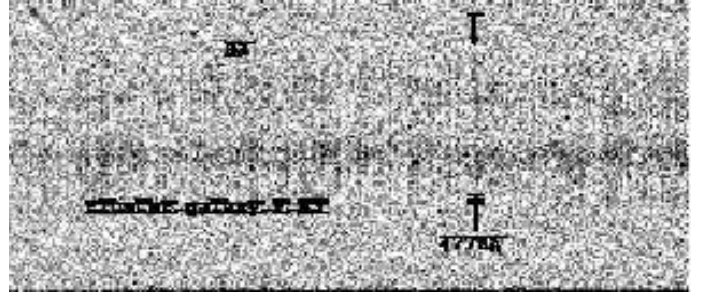


Fig. 10. Two dimensional spectra of two different images of the arc B: B2 (top) and B3+B4 (bottom). The arrows point the position of a faint emission line, visible in both spectra of B2 and B3+B4 images. The B3+B4 spectrum is contaminated by light from a nearby cluster galaxy. The slit was placed on the alignment of the B2 image with B3 and B4 (see Fig. 1).

$\text{CIV } 1549\text{\AA}$, which is a more likely case, then $z = 2.08$, a value which is still compatible with the z_{phot} at 2σ . Unfortunately, in this case $\text{Ly}\alpha$ is outside the spectral range observed. If the lens model in this region is responsible for the discrepancy, and the actual redshift of B is higher than $z \sim 1.4$, then the redshift prediction for the system C, $z = 2.3 \pm 0.1$, is also likely to be underestimated. Deeper spectroscopy in the I-z bands may allow to detect the $[\text{OII}]$ emission line, specially if the lensing prediction is correct.

Our spectrum of image C3 provides a fair estimate of the redshift of the multiple image C, which shows a blue continuum with absorption features identified as $\text{Ly}\alpha$ and $\text{CIV } 1549\text{\AA}$. The redshift derived from these two lines is $z=2.854$, which is fully compatible with the z_{phot} estimates. Figure 6 displays a comparison between the spectra

of C3 and that of a local starburst. Such a spectroscopic redshift is however much larger than the present lens prediction, but in concordance with the results obtained for the multiple image B. Clearly better data on B and C are required before deriving any strong conclusion.

6.5. The amplified galaxies V1, V2, V3, V4 and V5

Four other, high redshift, single-image galaxies were observed with FORS-1:

- V1 is the only source for which we could not identify a clear spectral feature, despite a long exposure time (2h47m) using two different slit configurations. This object is faint and has a blue SED. According to its z_{phot} determination, $z=1.13$, but no strong emission line was detected, in spite of the fact that [OII]3727Å is expected at $\lambda \sim 8000$ Å.
- V2 displays a single emission line, superimposed on a continuum spectrum, which leads to a redshift $z=1.2143$ when identified with [OII]3727Å. The z_{phot} determination is in good agreement with this spectroscopic redshift.
- The only clear spectral feature in the spectra of V3 is an emission line at $\lambda = 4776$ Å. The z_{phot} determination gives a 1σ interval ranging between 0.81 and 0.96, with a best fit at $z=0.84$. The most likely identification of this emission line is MgII(2798Å), leading to $z=0.706$, a value which is still compatible with the z_{phot} determination at 3σ . Unfortunately, the [OII]3727 Å line is expected to lie upon the atmospheric [OI] line at 6300 Å, thus it is hardly detected.
- The spectrum of V4 shows an emission line, with P-Cygni profile, and a blue continuum. According to its z_{phot} determination, it is either a high- z source, with $z=2.04$ (1σ error bar ranging between $z=2.0$ and $z=2.07$), or a $z=0.29$ foreground galaxy (or even a cluster member within the errors). In the first case, the emission line is identified to CIV 1549Å, leading to $z=2.050$. In the low- z case, the emission line is most likely identified with [OII]3727 Å, and in this case $z=0.272$, leading to $M_B = -17.19$. The latter identification is difficult to reconcile with the morphology of this object, as it appears on the HST images. In addition, the comparison between this spectrum and that of a local starburst allows to identify other significant absorption features, which reinforces the high- z identification (Fig. 6).
- V5 displays a single emission line, at $\lambda = 7724.4$ Å, and a relatively blue featureless continuum. According to its z_{phot} determination, the emission line can be identified with [OII]3727 Å, leading to $z=1.0726$.

6.6. Absolute Magnitudes in the spectroscopic sample

The revised mass model has been used to derive the magnification of each of the images. The absolute magnitudes M_B for these amplified galaxies are computed through a

direct scaling of the observed SED, taking into account the spectroscopic z , and using the best-fit templates from the Bruzual & Charlot code (Bruzual & Charlot 1993) to derive the k-corrections. The M_B values, corrected for amplification according to the revised NKSE model, are given in Table 5. The absolute magnitudes of these galaxies typically range from $M_B \sim -19$ to -22 , with a median value of -20.5 . In the cluster core, where the amplification is the highest, absolute magnitudes range between $M_B \sim -19$ and -21.5 . In particular, E and C, the two objects with confirmed redshifts in the interval $2.5 \lesssim z \lesssim 3.5$, are respectively 0.5 and 1.5 magnitudes fainter than the limiting magnitude of the Steidel et al (1999) sample at similar redshifts. In the case of S, the magnification corrected magnitude is close to the limiting value in conventional samples, but the magnification of ~ 2 magnitudes per image allows the obtention of spectra with higher signal-to-noise ratios.

6.7. Redshift distribution of lensed galaxies in the photometric sample

One of the main goals of this program is to recover the intrinsic properties of a very faint subsample of high- z lensed galaxies, undetectable otherwise, using deep images and z_{phot} , in order to investigate, in particular, their z distribution and luminosity function. We have obtained through *hyperz* the $N(z_{phot})$ distribution of arclets in the $1.2' \times 1.2'$ core of AC114, a region covered by all the images in Table 1. Fig. 11 displays the raw $N(z_{phot})$ distribution for the 148 objects considered in this region. This sample includes objects detected in at least 3 filters. For z_{phot} calculations, undetected objects in a given band have their flux in this band set to zero, with a flux error corresponding to the local limiting magnitude. Photometric errors are taken from SExtractor, with a threshold zeropoint error of 0.1 magnitudes. From this sample, we exclude all cluster-member candidates on the basis of their SEDs. Eight foreground and 81 background galaxies remain in the final sample, defined as objects excluded as cluster members to better than 90% confidence level, with $z \leq 0.2$ or $z \geq 0.4$. Forty-four galaxies are found at $1 \leq z \leq 7$ in a $1.2' \times 1.2'$ field centered on the cD galaxy. For comparison, the total number of such sources expected in this field, taking into account the depth of the survey, ranges from ~ 30 to 50 sources. The selection criteria allow that the background sample includes all the objects selected for spectroscopy in the cluster core.

For cluster lenses with well constrained mass distributions, as in the present case, it is possible to recover precisely the $N(z_{phot})$ and the absolute magnitude distributions of lensed galaxies by correcting the relative impact parameter on each redshift bin. We have used the NKSE corrected mass model to derive such distributions for the background sample of galaxies. Fig. 12 displays the lens corrected absolute magnitude M_B distribution versus redshift for the sources in the field of AC114. Up to $z \sim 4$,

Id.	z (spectra)	z (phot.)	Δz (phot.)	z (lensing)	Δm mag.	M_B	Comments
A1 A2	1.6912	2.04	1.27-2.80	1.67 ± 0.15	1.58(A1)	-20.5	
B2 B3							
							M_B with $z=1.50$
C3	2.854	2.76	2.67-2.91	2.1 ± 0.3	2.40	-20.8	
E1	3.34695	3.45	3.29-3.60	-	1.40	-20.6	
S2	1.86710	2.06	1.97-2.25	-	2.18	-21.2	
V1	?	1.13	1.05-1.22		1.43	-19.9	M_B based on z_{phot}
V2	1.2143	0.945	0.41-1.08		0.80	-20.9	
V3	0.706	0.84	0.81-0.96		0.48	-19.1	
V4	2.050	0.29/2.04	0.26-0.31/2.0-2.07		0.85	-21.4	
V5	1.0726	1.05	0.91-1.47		0.86	-20.7	
V6	0.40953	0.46	0.38-0.50		0.142	-19.5	
V7	0.56692	0.54	0.53-0.55		0.239	-21.7	
V8	0.58?	0.48	0.12-2.08		0.328	-20.2	
V9	0.41205	-	-		0.052	-20.8	
V10	0.80340	-	-		0.321	-21.7	
V11	0.38048	-	-		0.037	-19.6	
V12	0.72002	0.51	0.373-0.59		0.146	(-22.6)	
V13	0.71965	0.82	0.348-2.3		0.071	(-20.7)	
V14	0.90031	1.26	0.54-3.29		0.082	(-20.7)	
V15	0.90233	-	-		0.074	-22.7	
V16	0.89935 ?	-	-		0.067	-22.2	
V17	0.71169	-	-		0.040	-20.6	
V18	0.8135 ?	-	-		0.053	(-23.9?)	

Table 5. Characteristics of the background galaxies studied in AC114. Identifications are the same as in Table 2. M_B have been corrected for magnification Δm according to the revised NKSE model. The z_{lens} values are from NKSE(1998). Error bars in z_{phot} correspond to 1σ using also a B-image. M_B given in brackets correspond to objects for which the restframe B band has been extrapolated from the available photometry, using the best fit model. It is highly model dependent in the case of V18.

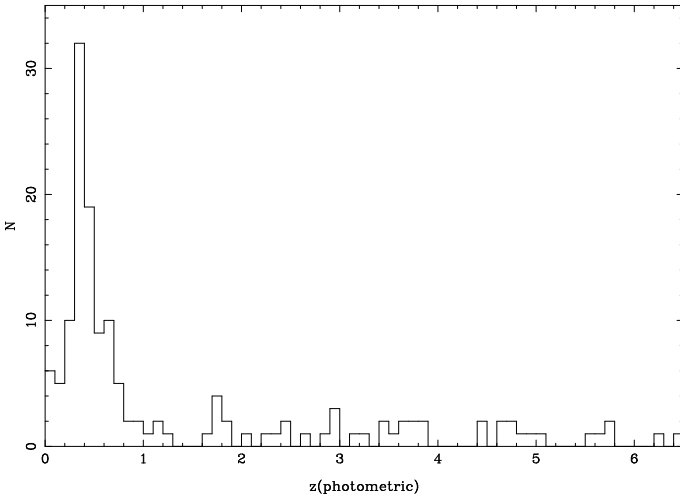


Fig. 11. Raw photometric redshift distribution of galaxies in the $1.2' \times 1.2'$ cluster core.

the restframe B band is well matched by the filters used here. The median value of M_B is -21.5 for the 44 galaxies at $1 \lesssim z \lesssim 7$, with typical values ranging between -19 and -23. In the $1 \lesssim z \lesssim 3.5$ redshift interval (23 galaxies),

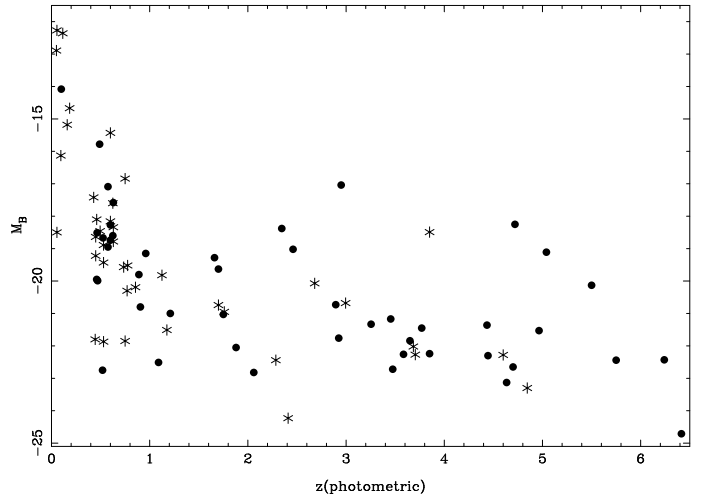


Fig. 12. Lens corrected absolute magnitude distribution versus redshift for sources in the $1.2' \times 1.2'$ cluster core. Black dots and stars correspond to objects with reduced $\chi^2 \leq 1.5$ and $\chi^2 > 1.5$, respectively.

the median M_B is -21.0. Thus, the spectroscopic sample is biased towards the most amplified sources in the central

region, and thus intrinsically fainter than the photometric sample. The median intrinsic luminosity increases to $M_B \sim -22$ for the $z \geq 3.5$ sample. Because of the small number of objects in the sample, this exercise is of limited interest for a single cluster, when using standard (not ultra-deep) imaging, but it is useful to illustrate the case.

7. Discussion

This study has allowed to improve the NKSE lensing model for the massive and well studied cluster AC114, mainly through the discovery of a new multiple-image system, the E-system. This discovery was driven by the identification of a very high- z galaxy in the core of AC114 thanks to deep multi-band images, and specifically through the photometric redshift technique. This multiple-image system was missed by a search of lensed objects in the high-resolution HST images due to its point-like appearance.

An indication of the precision that can be attained for the intrinsic luminosities of the background galaxies is obtained from the independent inferences, based on the revised mass model, that can be made from the photometry of the individual images belonging to a given multiple image system. The typical uncertainty in the magnification factor is ~ 0.3 magnitudes for most objects, and this gives an idea of the limitations arising from lens modelling when using gravitational telescopes.

The iterative optimization of the mass model together with feedback between the lens and photometric redshifts in this stage, makes highly desirable to have deep multi-band image. Thus, high-resolution images in addition to deep multi-band images are actually needed for the selection of high- z galaxy candidates and the obtention of sufficient constraints to establish a robust mass model. This could be done for a master list of clusters that could be made public through archives. Once the mass model is mature for a cluster, such as for AC114 now, deeper and higher resolution images, and occasional spectroscopy, should conduct to key information and new discoveries in the distant universe.

The galaxy cluster AC114, with its highly constrained gravitational-lens model, is a particularly powerful gravitational telescope for which further lensing studies can be undertaken, such as searching for distant supernovae (Sullivan et al 2000), distant Submm sources (Smail et al 1997) or Lyman- α emitters (Ellis et al, in preparation). By performing a very accurate mass modelling we can also expect to constraint the cosmological parameters (Ω , λ) using the method of Golse et al (2001).

The source responsible for the multiple image E at $z = 3.347$ is intrinsically faint, roughly the equivalent of the local $M_B^* + 0.5$ magnitudes. The presence of a relatively strong emission line, together with the gravitational magnification, has allowed us to obtain a spectroscopic redshift. This galaxy is intrinsically ~ 0.5 magnitudes fainter than the limiting value of the Steidel et al (1999) sample at similar redshifts. It has a bright core and at least two

faint extensions, similar to the morphology of the compact cores in the field sample of Steidel et al (1996a) at $2.5 \lesssim z \lesssim 3.5$. The main subclump displays a compact morphology, which is not resolved in width on the WFPC2 images, thus implying length scales of the order of $\sim 1 kpc$. Its morphology and the equivalent (rest frame) width of Ly α are similar to those of H5, one of the multiple images at $z=4.05$ identified in the core of A2390 (Pelló et al 1999), and also similar to the typical values observed by Hu et al (1998) in their sample of emission line galaxies at $z \sim 3$ to 6.

Six galaxies in our spectroscopic sample are found at $1 \lesssim z \lesssim 2.5$, a redshift domain which is relatively poorly known because of the lack of strong spectral features allowing to identify sources in this redshift interval. The gravitational amplification has allowed to identify such objects, and the precise redshift determination, using visible and near-IR spectrographs in 8-10m class telescopes, will allow a detailed study of the spectral energy distributions of these $z \geq 1$ galaxies. In particular, studies of the star formation rate history and of the permitted region in the age-metallicity-reddening parameter space, are now possible and will be presented in the future. The best example is the source S, for which a detailed spectroscopic study is presently in progress.

The median value of M_B is -21.5 for the photometric sample of galaxies at $1 \lesssim z \lesssim 7$, with typical values ranging between -19 and -23 . The median M_B is -21.0 in this sample, in the $1 \lesssim z \lesssim 3.5$ redshift interval, and it increases to $M_B \sim -22$ for the $z \geq 3.5$ sample. The spectroscopic sample in the cluster core is biased towards the most amplified sources, which are intrinsically fainter than the photometric sample, and it exhibits a median M_B of -20.5 in the $1 \lesssim z \lesssim 3.5$ redshift bin, with absolute magnitudes ranging between $M_B \sim -19$ and -21.5 . Lensed galaxies in this spectroscopic sample are found to be intrinsically fainter, between 0.5 and 1.5 magnitudes, than the limiting magnitudes in the present *blank field* surveys at $2 \lesssim z \lesssim 3.5$ (Steidel et al 1999). This gain in sensitivity towards low luminosity high- z objects, equivalent to an increase in collecting area by at least a factor of 2 to 3 (and up to a factor of ~ 10 in restricted regions of the source plane), is sufficiently large to allow a substantial improvement on our knowledge of the faintest and/or highest redshift galaxies.

8. Conclusions

In summary, we have successfully identified 23 galaxies in the background of AC114, 10 of them being high-redshift objects, with $0.7 \lesssim z \lesssim 3.5$, located on the cluster core. The main results of our spectroscopic survey, concerning multiple-image systems and the mass model of this cluster, are:

- We confirm the redshift $z=1.87$ of the gravitational pair S1/S2.

- The redshift of the multiple image system A has been measured: $z=1.69$, in excellent agreement with the lensing and photometric predictions.
- A new 5-image multiple system E at redshift $z=3.347$ is identified. We use this new strong constraint, together with the previously used multiple system S, to derive an improved mass model for AC114.
- The redshifts of the multiple images B and C are determined, however new and better quality data are needed to confirm them. So far, their current determinations are slightly larger than those predicted by the original NKSE, and still difficult to reconcile with the revised model.

Overall, these results show the validity of the approach and the good accuracy of the predictions of the lensing model, and clearly establish with great confidence a mass model for AC114: the revised NKSE model.

We have demonstrated the efficiency of a lensing/photometric approach to derive new samples of high- z galaxies, conditioned to the availability of high-resolution images and a fairly well determined mass model for the cluster-lens. All the highly magnified galaxies in the spectroscopic sample have $M_B \sim -21.5$ to -19 opening a way to study the faint end slope of the luminosity function in early epochs of the universe. In particular, the 2 objects (C,E) with spectroscopic $2.5 \lesssim z \lesssim 3.5$, are respectively 0.5 and 1.5 magnitudes fainter than the limiting magnitude of the Steidel et al (1999) survey at similar redshifts. We plan to continue efforts to gather a sample of very faint high- z lensed galaxies employing the z_{phot} technique described in this work, and to investigate their spectral energy distributions using visible and near-IR spectrographs in 8 or 10-m class telescopes. A galaxy sample of the proper size to study their luminosity function will require observations and analyses, similar to the one presented here for AC114, of about ten massive cluster-lenses.

Acknowledgements. We are grateful to M. Bolzonella, G. Bruzual, M. Dantel-Fort, G. Mathez and D. Schaerer for useful discussions on this particular program. We would like to thank Dr. W. J. Couch for providing his deep B image of AC114, and Dr. C. Leitherer for allowing the use of the NGC 4214 spectrum. LEC was partially supported by FONDECYT grant 1970735. Part of this work was supported by the French *Centre National de la Recherche Scientifique*, by the French *Programme National de Cosmologie* (PNC), and the TMR *Lensnet* ERBFMRXCT97-0172 (<http://www.ast.cam.ac.uk/LoA/lensnet>) and the ECOS SUD Program. Based on observations collected at the European Southern Observatory, Chile (ESO N 64.O-0439), and with the NASA/ESA Hubble Space Telescope, which is operated by STScI for the Association of Universities for Research in Astronomy, Inc., under NASA contract NAS5-26555.

References

Abell, G.O., Corwin, H.G.Jr, Olowin, R.P., 1989, ApJS 70, 1.
 Altieri, B., Metcalfe, L., Kneib, J.-P., McBreen, B., Aussel, H., Biviano, A., Delaney, M., Elbaz, D., Leech, K., Lemonon,

L., Okumura, K., Pelló, R., Schulz, B., 1999, A&A 343, L65
 Arnouts, S., Cristiani, S., Moscardini, L., Matarrese, S., Lucchin, F., Fontana, A., Giallongo, E. 1999, MNRAS 310, 540
 Barger, A.J., Aragón-Salamanca, A., Ellis, R.S., Couch, W.J., Smail, I., Sharples, R.M., 1996, MNRAS 279, 1
 Bertin, E., Arnouts, S. 1996, A&ASS 117, 393
 Bézecourt, J., Soucail, G., Ellis, R. S., Kneib, J.-P., 1999, A & A 351, 433
 Bolzonella, M., Miralles, J.M., Pelló, R., 2000, A & A 363, 476
 Broadhurst T. J., 1995, preprint astro-ph/9511110
 Bruzual, G., Charlot, S., 1993, ApJ 405, 538
 Ebbels, T.M.D., Ellis R.S., Kneib J.P., Le Borgne J.-F., Pelló R., Smail I., Sanahuja B., 1998, MNRAS 295, 75
 Fernández-Soto, A., Lanzetta, K.M., Yahil, A. 1999, ApJ 513, 34
 Fort, B., Mellier, Y., Dantel-Fort, M., 1997, A & A 321, 353
 Furusawa, H., Shimasaku, K., Doi, M., Okamura, S. 2000, ApJ 534, 624
 Giallongo, E., D’Odorico, S., Fontana, A., Cristiani, S., Egami, E., Hu, E., McMahon, R.G. 1998, AJ 115, 2169
 Golse, G., Kneib, J. P., Soucail, G., 2001, submitted to A & A, astro-ph/0103500
 Gwyn, S.D.J., Hartwick F.D.A. 1996, ApJ 468, L77
 Hu, E. M., Cowie L. L., McMahon R. G., 1998, ApJ 502, L99
 Ivison, R. J., Smail, I., Barger, A. J., Kneib, J.-P., Blain, A. W., Owen, F. N., Kerr, T. H., Cowie, L. L. 2000, MNRAS 315, 209
 Kneib, J.-P., 1993, Thesis, U. Paul-Sabatier
 Kneib, J.-P., Mathez, M., Fort, B., Mellier, Y., Soucail, G., Longaretti, Y., 1994, A&A 286, 701.
 Kneib, J.-P., Ellis R.S., Smail I., Couch, W.J., Sharples, R., 1996, ApJ 471, 643
 Lanzetta, K.M., Yahil, A., Fernández-Soto, A. 1996, Nature 381, 759
 Leitherer, C., Vacca, W. D., Conti, P. S., Filippenko, A.V., Robert, C., Sargent, W. L. W. 1996, ApJ 465, 717
 Mayen, C., Soucail, G., 2000, A&A 361, 415
 Metcalfe, L., Altieri, B., McBreen, B., Kneib, J.-P., Delaney, M., Biviano, A., Kessler, M.F., Leech, K., Okumura, K., Schulz, B., Elbaz, D., Aussel, H., 1999, In "The Universe as seen by ISO", eds.: P.Cox, M.F.Kessler, ESA Publication Division, ESTEC, Noordwijk, NL, astro-ph/9901147
 Mobasher, B., Rowan-Robinson, M., Georgakakis, A., Eaton, N. 1996, MNRAS 282, L7
 Natarajan, P., Kneib, J.p., Smail, I., Ellis, R.S., 1998, ApJ 499, 600 (NKSE)
 Pelló, R., J.-P. Kneib, J.-F. Le Borgne, J. Bezecourt, T. M. Ebbels, I. Tijera, G. Bruzual, J. M. Miralles, I. Smail, G. Soucail, T. J. Bridges 1999a, A&A 346, 359,
 Pelló, R., Kneib, J.-P., Bolzanella, M., Miralles, J.-M., 1999b, Conference Proceedings of the "Photometric Redshifts and High Redshift Galaxies", April 28-30, 1999, Pasadena, astro-ph/9907054.
 Sawicki, M.J., Lin, H., Yee, H.K.C. 1997, AJ 113, 1
 Smail, I., Ellis, R. S., Fitchett, M. J., Norgaard-Nielsen, H. U., Hansen, L., Jorgensen, H. E., 1991, MNRAS 252, 19
 Smail, I., Couch, W.J., Ellis, R.S., Sharples, R.M., 1995, ApJ 440, 501.
 Smail, I., Ivison, R. J., Blain, A.W., 1997, ApJ 490, L5.
 Steidel C.C., Hamilton, D., 1993, AJ 105, 2017
 Steidel C.C., Giavalisco M., Pettini M., Dickinson M., Adelberger K., 1996a, ApJ 462, L17

- Steidel C.C., Giavalisco M., Dickinson M., Adelberger K.,
1996b, AJ 112, 352
- Steidel C.C., Adelberger K., Dickinson M., Giavalisco M.,
Pettini M., Kellogg, M., 1998, ApJ 492, 428
- Steidel, C.C., Adelberg, K. L., Giavalisco, M., Dickinson, M.,
Pettini, M., 1999, ApJ 519, 1
- Sullivan, M., Ellis, R., Nugent, P., Smail, I., Madau, P., 2000,
MNRAS 319, 549

This figure "lowz3.jpg" is available in "jpg" format from:

<http://arxiv.org/ps/astro-ph/0104477v1>

This figure "ac114_core.jpg" is available in "jpg" format from:

<http://arxiv.org/ps/astro-ph/0104477v1>

This figure "highz.jpg" is available in "jpg" format from:

<http://arxiv.org/ps/astro-ph/0104477v1>